



**HAL**  
open science

## Size evolution of Eu(III)-fulvic acid complexes with pH, metal, and fulvic acid concentrations: implications for modelling of metal-humic substances interactions

Yasmine Kouhail, Pascal E Reiller, Laurent Vio, Marc F Benedetti

### ► To cite this version:

Yasmine Kouhail, Pascal E Reiller, Laurent Vio, Marc F Benedetti. Size evolution of Eu(III)-fulvic acid complexes with pH, metal, and fulvic acid concentrations: implications for modelling of metal-humic substances interactions. *Environmental Chemistry*, 2024, 21 (2), pp.EN23108. 10.1071/EN23108 . hal-04549318

**HAL Id: hal-04549318**

**<https://cnrs.hal.science/hal-04549318>**

Submitted on 17 Apr 2024

**HAL** is a multi-disciplinary open access archive for the deposit and dissemination of scientific research documents, whether they are published or not. The documents may come from teaching and research institutions in France or abroad, or from public or private research centers.

L'archive ouverte pluridisciplinaire **HAL**, est destinée au dépôt et à la diffusion de documents scientifiques de niveau recherche, publiés ou non, émanant des établissements d'enseignement et de recherche français ou étrangers, des laboratoires publics ou privés.

1 **Size evolution of Eu(III)-fulvic acid complexes with pH, metal, and**  
2 **fulvic acid concentrations: implications for modelling of metal-humic**  
3 **substances interactions.**

4 **Yasmine Kouhail<sup>1,2</sup>, Pascal E. Reiller<sup>1</sup>, Laurent Vio<sup>1,3</sup>, Marc F. Benedetti<sup>2\*</sup>**

5 <sup>1</sup> Université Paris-Saclay, CEA, Service de Physico-Chimie (SCP), F-91191, Gif-sur-Yvette, France.

6 <sup>2</sup> Université Paris Cité, Institut de Physique du Globe de Paris, CNRS, F-75005 Paris, France

7 <sup>3</sup> Present address: CEA, DG/CEACAD/D3S/SPR/LANSE, Cadarache, Saint-Paul-lès-Durance  
8 Cedex, France

9 **\* Correspondence:**

10 Marc F. Benedetti

11 benedetti@ipgp.fr

12 Present address: Karlsruher Institut für Technologie (KIT), Institut für Nukleare Entsorgung (INE),  
13 Hermann-von-Helmholtz Platz 1, D-76344 Eggenstein-Leopoldshafen, Germany

14

15 **Keywords: Humic substance, Europium, NICA-Donnan, Modeling, Hydrodynamic radius**

16 **Abstract**

17 **1**

18 **Abstract:**

19 2 Rationale: Humic substances (HS), including humic (HA) and fulvic (FA) acids, play a vital  
20 role in environmental systems, particularly in the sequestration and transport of trace metals.  
21 While existing models like the NICA-Donnan model have illuminated metal-HS interactions,  
22 the impact of HS concentration on these interactions remains insufficiently explored.

23 3 Methodology: This study centers on Suwannee River fulvic acid (SRFA) and investigates how  
24 its concentration influences the dimensions and electrostatic characteristics of SRFA  
25 complexes, utilizing europium(III) (Eu(III)) as a representative metal cation. The employed  
26 methodology involves Taylor dispersion analysis (TDA) with capillary electrophoresis to  
27 determine diffusion coefficients (D) and hydrodynamic radii (RH) of SRFA and Eu(III)-SRFA  
28 complexes. The NICA-Donnan model is employed to estimate site densities, intrinsic  
29 heterogeneity, and Donnan potential ( $\psi_D$ ).

30 4 Results: The RH values for SRFA and Eu(III)-SRFA complexes consistently fall between 0.78  
31 and 1.03 nm, indicating that pH and SRFA concentration minimally affect complex size.  
32 Donnan volume calculations based on RH align well with the NICA-Donnan model. The  
33 results reveal changes in electrostatic properties, particularly the Boltzmann factor ( $\chi$ ), which is  
34 sensitive to SRFA concentration, exhibiting more pronounced effects in trivalent cation-  
35 containing SRFA complexes.

36 5 Discussion: The study underscores that the concentration of HS, such as SRFA, significantly  
37 influences the size and electrostatic attributes of SRFA complexes, potentially impacting the  
38 behavior of other cations in environmental systems, including iron and aluminum. The findings  
39 highlight the importance of the metal/HS sites ratio in determining complex size and  
40 electrostatic properties, providing valuable insights into the behavior of natural organic matter  
41 in diverse environmental contexts. The discussion emphasizes the need for further research to  
42 explore the influence of different cations on HS structures across a broader concentration range.

## 43 6 Introduction

44 Humic substances (HS), mainly composed of humic (HA) and fulvic (FA) acids, are ubiquitous in  
45 the environment and are known to play an important role in the binding and transport of trace metals  
46 such as rare earth elements (McCarthy *et al.* 1998a, McCarthy *et al.* 1998b, Bryan *et al.* 2012). Because  
47 of HS heterogeneity, it is very difficult to determine their structure, which is strongly related to their  
48 reactivity. A wide variety of models (Benedetti *et al.* 1996, Tipping 1998, Kinniburgh *et al.* 1999,  
49 Hummel *et al.* 2000, Tipping *et al.* 2011) can describe metal-HS interactions. One of the widely used  
50 model, i.e. NICA-Donnan model (Benedetti *et al.* 1996, Kinniburgh *et al.* 1999), allows accounting for  
51 heterogeneity of HS, metal loading, pH, and ionic strength effects—and also to have a link on size  
52 evolution (Benedetti *et al.* 1996) — considering HS as a continuous distribution of groups of sites.

53 Cations, mostly divalent and trivalent, are known to play a role in supramolecular associations and  
54 organization of humic substances (von Wandruszka *et al.* 1997, Piccolo 2002, Sutton and Sposito 2005,  
55 Kunhi Mouvenchery *et al.* 2012, Kouhail *et al.* 2016), thus they can impact the size of HS entities  
56 (Benedetti *et al.* 1996). The effect of Eu(III), as a representative of lanthanides, on the aggregation of  
57 HA was shown (Plaschke *et al.* 2002, Plaschke *et al.* 2004, Naber *et al.* 2006), but the effect of HS  
58 concentration received little attention. A previous study on Suwannee River fulvic acid (SRFA)  
59 interactions with Eu(III) (Kouhail *et al.* 2016) raised some issues on supramolecular associations of  
60 FA, and the role of Eu in these associations. One of the hypotheses is that there might be a change in  
61 spatial organization of Eu-SRFA complexes with  $C_{\text{SRFA}}$ . The Eu(III) chemical environment evolution  
62 with  $C_{\text{SRFA}}$  was also proved to be ionic strength dependent. These observations suggested that in  
63 addition to short range interactions, i.e. intra-particulate complexation, there might be interactions at a

64 longer range, i.e. inter-particulate repulsion, between particles that are complexing Eu(III) at high  $C_{\text{SRFA}}$   
65 (Kouhail *et al.* 2016). Such inter-particulate interactions are not yet accounted for in the existing  
66 models describing metal interactions with HS.

67 Within the NICA-Donnan model framework (Benedetti *et al.* 1996, Kinniburgh *et al.* 1999), the  
68 Donnan volume,  $V_D$ , is optimized to build the acid-base titration master curves (MCs), and decreases  
69 with ionic strength following an empirical relationship (Benedetti *et al.* 1996). The Donnan potential,  
70  $\psi_D$ , inside this volume is assumed negative and constant inside the particle and nil outside. It can be  
71 calculated from the ratio of the activity of ions inside and outside the Donnan gel, and from the charge  
72 density inside the gel (Benedetti *et al.* 1996). The increase of Eu(III) association at high  $C_{\text{SRFA}}$  with  
73 ionic strength could then be linked to an apparent decrease of  $V_D$  and/or  $\psi_D$  (Kouhail *et al.* 2016). Since  
74  $\psi_D$  cannot be easily measured, the variation on Donnan volumes *vs.* pH, HS, and metal concentrations  
75 should be investigated in a first step. The verification of this hypothesis implies the determination of  
76 Donnan volumes of Eu(III)-SRFA complexes for varying experimental conditions. Determination of  
77  $V_D$  can be approached through the measurement of an average hydrodynamic radius,  $R_H$ , of the  
78 complex (Avena *et al.* 1999).

79 Taylor dispersion analysis (TDA) using a capillary electrophoresis (CE) instrument appears as an  
80 efficient tool for the characterization of HS samples under environmental conditions (d'Orlyé and  
81 Reiller 2012). This technique enables to determine the diffusion coefficients,  $D$ , of solutes. It relies on  
82 the specific dispersion profile of a solute plugged in a laminar Poiseuille flow, subjected to the  
83 combined effect of diffusion and convection. From the diffusion coefficients,  $R_H$  values of SRFA  
84 particles and Eu(III)-SRFA complexes can be estimated using the Stokes-Einstein equation.

85 In order to address the inter-particulate repulsion between particles that are complexing Eu(III) at  
86 varying fulvic acid concentration, in this study, we will use SRFA as a proxy for HS reactivity and we

87 propose to determine the  $R_H$  of Eu(III)-SRFA complexes at varying pH, Eu(III) and SRFA  
88 concentrations.

## 89 7 Material and methods

### 90 7.1 Reagents and Chemicals

91 Europium(III) stock solution ( $10^{-4}$  mol/L) was obtained from the dissolution of  $\text{Eu}_2\text{O}_3$  (Johnson  
92 Matthey, 99.99%) in  $\text{HClO}_4$ . All solutions were prepared using milli-Q water from a Direct Q3  
93 Millipore. Suwannee River fulvic acid (2S101F) was purchased from the International Humic  
94 Substances Society (IHSS, St. Paul, MN, USA) and used as received, and concentration ranged from  
95 30 to 500 mg/L. SRFA was dissolved in a pH 10 solution and laid to rest overnight. The SRFA samples  
96 were then adjusted to the desired pH value. The ionic strength was fixed with  $\text{NaClO}_4$  (Sigma Aldrich,  
97 >98%) at 0.1 M. The desired Eu(III) aliquot from the stock solution was added and the pH values were  
98 fixed at 4, 6, and 7 by the addition of small amounts of freshly prepared 0.1 M NaOH and/or  $\text{HClO}_4$ .  
99 Measurements were done using a pH meter Seven Easy (Mettler Toledo) with a combined glass  
100 electrode Inlab micro, filled with  $\text{NaClO}_4$  3M to avoid  $\text{KClO}_4$  precipitation in the frit of the electrode  
101 with the original KCl filling. The electrode was calibrated externally using commercial buffer solutions  
102 (pH 4.01, 7.01, and 10.00) with an uncertainty better than 0.08.

### 103 7.2 Capillary electrophoresis instrument

104 Taylor dispersion analysis (TDA) on a capillary electrophoresis instrument was used to determine  
105 diffusion coefficients and  $R_H$  values of SRFA particles and Eu(III)-SRFA complexes at pH 4, 6, and 7,  
106 at  $C_{\text{Eu(III)}}$  of 1 and 10  $\mu\text{M}$ . TDA was performed on a 7100 Agilent CE instrument (Agilent, Germany).  
107 Capillaries used were bare silica tubing with dimensions of 60.8 cm  $\times$  50  $\mu\text{m}$  and a detection window  
108 at 52.6 cm. New capillaries were conditioned by successive flushes: 1 M NaOH for 30 min; 0.1 M  
109 NaOH for 30 min; deionized water for 30 min. Between each run, capillaries were rinsed with 0.1 M  
110 HCl for 6 min; 0.1 M NaOH for 6 min; 0.1 M  $\text{NaClO}_4$  for 6 min. The inlet end of the capillary was

111 moved into the vial containing the sample. Experiments were done using a mobilization pressure of 50  
 112 mbar and the mobile phase was composed of the same electrolyte as in the HS sample (0.1 M NaClO<sub>4</sub>  
 113 at pH value equal to the sample pH). The temperature of the coolant liquid was set at 25 °C and the  
 114 detection wavelength for the UV-absorbance detector was set at 214 nm. All samples were run 3 times  
 115 and diffusion coefficients and R<sub>H</sub> were reported.

116 One can recall that in TDA no potential is applied during experiments.

### 117 7.3 Theory

#### 118 7.3.1 Taylor dispersion analysis data treatment

119 TDA theory has already been described in d'Orlyé *et al.* (2008) and references therein. The  
 120 convection diffusion equation for a front concentration profile is defined by the following equation:

$$\frac{\bar{C}}{\bar{C}_0} = \frac{1}{2} + \frac{1}{2} \operatorname{erf} \left[ \frac{(t - t_R)}{\sqrt{2\sigma^2}} \right] \quad (1)$$

121 with  $\bar{C}$  the mean solute concentration across the cross-section of the capillary as function of time at a  
 122 fixed position along the capillary axis,  $\bar{C}_0$  the concentration of the front,  $t_R$  the mean residence time of  
 123 the solute in the capillary until it reaches the detector, and  $\sigma^2$  is the temporal variance of the elution  
 124 profile. The diffusion along the axis of the capillary is assumed negligible. The  $\sigma^2$  value is usually  
 125 estimated by fitting the elution peak;  $\sigma^2$  is related to the dispersion coefficient,  $k$ , and to the mean  
 126 velocity of the fluid  $u$ .

$$\sigma^2 = \frac{2kt_R}{u^2} \quad (2)$$

127 The dispersion coefficient,  $k$ , can be determined by Taylor's theory (Taylor 1953), extended later by  
 128 Aris (1956):

$$k = D + \frac{R_c^2 u^2}{48D} \quad (3)$$

129 where  $D$  is the analyte diffusion coefficient and  $R_c$  is the capillary radius.

130 The mean residence time of the solute in the capillary  $t_R$ , has to be higher than the characteristic  
 131 diffusion time of the solute in the cross section of the capillary:

$$\tau = \frac{Dt_R}{R_C^2} > 1.4 \quad (4)$$

132 where  $\tau$  is a dimensionless residence time;

133 The Peclet number,  $P_e$ , has to be higher than 69 for the axial diffusion to be negligible compared to  
 134 convection:

$$P_e = \frac{uR_C}{D} > 69 \quad (5)$$

135 The diffusion coefficient can be determined using the following equation:

$$D = \frac{R_C^2 t_R}{24\sigma^2} \quad (6)$$

136 where  $t_R$  and  $\sigma^2$  are obtained by non-linear fitting of the UV detector signal at 214 nm to Eq. (1) using  
 137 the Solver from Microsoft Excel software. The uncertainties on the fitting parameters were obtained  
 138 using the SolverAid macro (de Levie 2004).

139 The  $R_H$  values for SRFA are then calculated using the Stokes-Einstein equation:

$$D = \frac{k_B T}{6\pi\eta R_H} \quad (7)$$

140 where  $k_B$  is the Boltzmann constant,  $T$  is the temperature (in K),  $\eta$  is the fluid viscosity ( $\text{kg}\cdot\text{s}^{-1}\cdot\text{m}^{-1}$ ) and  
 141  $R_H$  is the Stokes radius.

### 142 7.3.2 NICA Donnan model

143 The NICA-Donnan model merges the Non-Ideal Competitive Adsorption (NICA) model with a  
 144 continuous distribution of sites, and a Donnan potential description to account for electrostatic  
 145 interactions within the structure of HS. The model accounts for sites heterogeneity, non-ideality of the  
 146 metal-HS complexation, competition between metals (Eq. 8) and electrostatic interactions (Eq. 9, and  
 147 Eq. 10) (Benedetti *et al.* 1996).

$$Q_i = Q_{\max,1} \frac{n_{i,1}}{n_{H^+,1}} \frac{(\tilde{K}_{i,1} C_{D,i})^{n_{i,1}}}{\sum_j (\tilde{K}_{j,1} C_{D,j})^{n_{j,1}}} \frac{[\sum_j (\tilde{K}_{j,1} C_{D,j})^{n_{j,1}}]^{p_1}}{1 + [\sum_j (\tilde{K}_{j,1} C_{D,j})^{n_{j,1}}]^{p_1}} \quad (8)$$

$$+ Q_{\max,2} \frac{n_{i,2}}{n_{H^+,2}} \frac{(\tilde{K}_{i,2} C_{D,i})^{n_{i,2}}}{\sum_j (\tilde{K}_{j,2} C_{D,j})^{n_{j,2}}} \frac{[\sum_j (\tilde{K}_{j,2} C_{D,j})^{n_{j,2}}]^{p_2}}{1 + [\sum_j (\tilde{K}_{j,2} C_{D,j})^{n_{j,2}}]^{p_2}}$$

148 where  $Q_{\max,1}$ , and  $Q_{\max,2}$  are site densities of the two distribution of sites of SRFA,  $p_1$  and  $p_2$  are the  
 149 widths of the distributions of sites and are representing the intrinsic heterogeneity,  $n_i$  is the non-ideality  
 150 parameter, and  $\tilde{K}_{i,1}$  is the median affinity for low-affinity type of sites—so-called carboxylic  $S_1$ —and  
 151  $\tilde{K}_{i,2}$  is the median affinity for high-affinity type of sites—so-called phenolic  $S_2$ .

152 Within the NICA-Donnan model framework (Benedetti *et al.* 1996, Kinniburgh *et al.* 1999), the  
 153 Donnan volume  $V_D$  is optimized to build the acid-base titration master curves, and decreases with ionic  
 154 strength,  $I$ , following an empirical relationship (Benedetti *et al.* 1996). The Donnan potential  $\psi_D$  inside  
 155 this volume is assumed negative and constant inside, and nil outside the particle. It can be calculated  
 156 from the activity of ions inside ( $a_{i,D}$ ) and outside ( $a_i$ ) the Donnan gel – related by a Boltzmann factor  $\chi$   
 157 – and from the charge density,  $q$ , inside the gel.

$$a_{i,D} = \chi^{z_i} a_i = a_i \exp\left(-\frac{e\psi_D}{kT}\right) = a_i \exp\left(-\frac{z_i F}{RT} \psi_D\right) \quad (9)$$

$$\frac{q}{V_D} + \sum_i z_i (a_{i,D} - a_i) = 0 \quad (10)$$

158 For monovalent salts, it follows from Eq. (9) that

$$\chi^- = \frac{1}{\chi^+} \quad (11)$$

159 The combination of Eqs. (9), (10), and (11) gives

$$\frac{q}{V_D} = c_s \left( \chi^+ - \frac{1}{\chi^+} \right) \quad (12)$$

160 where  $c_s$  is the salt concentration.

161 The latter equation can also be written as

$$(\chi^+)^2 + \left(-\frac{q}{V_D c_s}\right)\chi^+ - 1 = 0 \quad (13)$$

162 which has only one physically realistic solution since  $\chi^+$  can only be positive.

163 In order to understand the effect of Eu(III) speciation changes on the size of the organic colloids,  
 164 modeling was performed using ECOSAT software (Keizer and van Riemsdijk 1994), which includes  
 165 speciation with inorganic ligands and HS through the NICA-Donnan model (Kinniburgh *et al.* 1999).  
 166 Milne *et al.* (2001) proposed generic data for HA and FA complexation with protons, and several  
 167 metals of interest (Milne *et al.* 2003). The inorganic side reactions of Eu(III) with OH<sup>-</sup> from Hummel  
 168 *et al.* (2002) are implemented in the ECOSAT database. Site densities of the two distribution of sites  
 169 of SRFA, parameters representing the intrinsic heterogeneity, and generic proton parameters for low-  
 170 affinity type of sites and high-affinity type of sites (Kouhail *et al.* 2016) proposed by Milne *et al.* (Milne  
 171 *et al.* 2001, Milne *et al.* 2003) are recalled in Table 1.

## 172 **8 Results and discussion**

### 173 **8.1 Estimated $R_H$ with TDA**

174 Taylor dispersion analysis using a capillary electrophoresis instrument is used to determine the  
 175 average diffusion coefficients of SRFA and Eu(III)-SRFA complexes at varying pH,  $C_{Eu}$ , and  $C_{SRFA}$   
 176 given in Table 2. Non-linear least-square fitting of Eq (1) are done for the front concentration profiles  
 177 considering mono-modal diffusion coefficient distributions. Experimental front concentration profile  
 178 and the Taylogram of an Eu-SRFA complex at pH 4 are presented in Figure 1. For different HS  
 179 samples, d'Orlyé and Reiller (2012) pointed out that the fitting of the front concentration profile can  
 180 be improved by considering a bi-modal diffusion coefficient distribution—same retention time  $t_R$ , but  
 181 different proportions  $x_1$  and  $x_2$ , with  $x_1+x_2=100\%$ , and different temporal variances  $\sigma_1$  and  $\sigma_2$ —for HS  
 182 samples except for SRFA samples. In this work, we corroborate this observation since a bi-modal  
 183 distribution is not improving the fitting, and statistical parameters (F) are not different using either a  
 184 mono or a bi-modal distribution for our SRFA samples. From  $D$  mean values,  $R_H$  values of

185 Eu(III)-SRFA complexes are then estimated using Eq (7). The obtained  $R_H$  values vs.  $C_{SRFA}$  at pH 4, 6,  
186 and 7, for SRFA and for Eu-SRFA samples with  $C_{Eu}$  of 1 and 10  $\mu\text{M}$  (Figure 2), are between 0.78 and  
187 1.03 nm. These  $R_H$  values are very close to the ones determined for the same SRFA sample with TDA,  
188 i.e.  $R_H = 0.88$  nm for  $C_{SRFA}$  of 500  $\text{mg}_{SRFA}/\text{L}$  at pH 10 and different ionic strengths. (d'Orlyé and Reiller  
189 2012) This suggests that there seems to be no major changes in  $R_H$  with pH at quite high  $C_{SRFA}$ .

190 Almost all techniques for size determinations have been applied for HS samples, but each technique  
191 is limited by their observation volumes, which are not necessarily comparable with each other.  
192 However, these nanometric sizes were commonly observed for various HS samples using TDA  
193 (d'Orlyé and Reiller 2012), vapor pressure osmometry (Aiken and Malcolm 1987, Chin *et al.* 1994,  
194 Peuravuori and Pihlaja 1997, Peuravuori *et al.* 2007), small angle neutron (SANS) or X-ray scattering  
195 (SAXS) (Österberg *et al.* 1994, Diallo *et al.* 2005), flow field flow fractionation (FFFF) (Bouby *et al.*  
196 2002, Bouby *et al.* 2011), fluorescence correlation spectroscopy (FCS) (Hosse and Wilkinson 2001,  
197 Domingos *et al.* 2009), or atomic force microscopy (AFM) (Baalousha and Lead 2007). We can also  
198 notice that  $R_H$  of SRFA calculated with the master curve approach in Benedetti *et al.* (1996) is also  
199 consistent with these experimental data since it was estimated at 1 nm at  $I = 0.1$  M. Similarly, the  $R_H$   
200 of SRFA calculated with the master curve approach from Tesfa *et al.* (2022) are quite consistent with  
201 the present ones and further demonstrate that estimation of  $V_D$  values with the approach from Benedetti  
202 *et al.* (1996) are quite good.

203 At pH 4 and  $C_{Eu(III)} = 1 \mu\text{M}$ , we could not evidence a significant change in  $R_H$  values with  $C_{SRFA}$   
204 between SRFA and Eu(III)-SRFA. Conversely, at pH 6 and 7 there is a small, but significant, decrease  
205 in  $R_H$  values with  $C_{SRFA}$ , which was not observed by Lead *et al.* (2000). For  $C_{SRFA}$  between 30 and 100  
206  $\text{mg}_{SRFA}/\text{L}$ ,  $R_H$  seem to be higher at pH 6 and 7 than at pH 4. It could be explained by molecular  
207 expansion due to repulsive forces amongst charged groups with pH (Lead *et al.* 2000).

208 At  $C_{\text{Eu(III)}} = 10 \mu\text{M}$ , a quite different compartment is observed for Eu(III)-SRFA: the  $R_{\text{H}}$  values are  
 209 almost identical at a  $C_{\text{SRFA}}$  higher than  $300 \text{ mg}_{\text{SRFA}}/\text{L}$ , regardless of pH and  $C_{\text{Eu}}$ , while  $R_{\text{H}}$  are smaller  
 210 for the lower concentrations. These small decreases in  $R_{\text{H}}$  observed with increasing  $C_{\text{Eu}}$  are most likely  
 211 indicating a change in the complex's structures that can be molecular compression due to a decrease  
 212 in intramolecular repulsions.

## 213 8.2 Donnan volume calculations

214 Donnan volumes are calculated using  $R_{\text{H}}$  obtained from TDA experiments with Eq. (14),

$$V_D = \frac{4\pi R^3 N_a}{3M_w} - \frac{1}{\rho_{\text{HS}}} \quad (14)$$

215 where  $M_w$  is an average molecular weight,  $N_a$  is the Avogadro's number, and  $\rho_{\text{HS}}$  is the dry bulk density.  
 216 In agreement with d'Orlyé and Reiller (2012), we use  $M_w = 829 \text{ g/mol}$  for the calculations (Benedetti  
 217 *et al.* 1996, Moulin *et al.* 2001, Plancque *et al.* 2001, Benedetti *et al.* 2002, Piccolo and Spiteller 2003).  
 218 One can stress that, first, the choice of a particular  $M_w$  is implying a  $V_D$  value, and second, that  $V_D$  is  
 219 decreasing when  $M_w$  increases.

220 Avena *et al.* (1999) studied the possibility to use the measured  $R_{\text{H}}$  as Donnan radius and came to the  
 221 conclusion that the obtained Donnan volumes were too small and are not satisfying for the MC  
 222 approach (De Wit *et al.* 1990). This observation could come from the use of different concepts that do  
 223 not provide the same  $R_{\text{H}}$  values. The Donnan model is valid when the size of the gel is large compared  
 224 to the Debye length but experimentally,  $R_{\text{H}}$  of HS are close to the Debye length or even smaller (Avena  
 225 *et al.* 1999). Saito *et al.* (Saito *et al.* 2005, Saito *et al.* 2009) compared the empirical relationship used  
 226 in the NICA-Donnan model with the option of a Donnan radius equals to the sum of the calculated  $R_{\text{H}}$   
 227 value and the Debye length  $\kappa^{-1}$ ,

$$\kappa^{-1} = \sqrt{\frac{\varepsilon_r \varepsilon_0 k_B T}{2N_a e^2 I}} \quad (15)$$

228 with  $I$  the ionic strength,  $\varepsilon_0$  the permittivity of free space,  $\varepsilon_r$  the water dielectric constant,  $k_B$  is the  
 229 Boltzmann constant,  $T$  the temperature (K), and  $e$  the elementary charge.

230 These two options to account for  $V_D$  in models gave adequate MCs (Saito *et al.* 2005). Donnan  
 231 volumes of SRFA,  $^{SRFA}V_D$ , and Eu-SRFA,  $^{Eu-SRFA}V_D$ , calculated using Eq. (14) are presented in Table 2.

232 The  $V_D$  values calculated from TDA experiments with  $R = R_H$  are ranging from 0.98 to 2.90 L/kg.  
 233 These values are in agreement with the  $V_D$  calculated with the empirical relationship (Benedetti *et al.*  
 234 1996)— $b = 0.57$  for a generic fulvic acid (Milne *et al.* 2001) leading to  $V_D = 1.38$  L/kg. The  $V_D$  values  
 235 calculated with  $R = R_H + \kappa^{-1}$  are ranging from 15.9 to 24.0 L/kg, which seems unlikely for fulvic acids.  
 236 Fulvic acids intrinsic viscosities  $[\eta]$  measurements support this point since they are related to  $R_H$   
 237 according to Eq. (16) (Kawahigashi *et al.* 2005):

$$[\eta] = 2.5 \times \left( \frac{4\pi R_H^3 N_a}{3M_w} \right)^{1/3} \quad (16)$$

238 Avena *et al.* (1999) reported intrinsic viscosities of FA equals to 5-10 L/kg for  $I = 0.1$  M—meaning  
 239  $R_H$  of 0.87-1.1 nm and  $V_D$  of 1.5-3.5 L/kg. Ghosh and Schnitzer (1980) reported values in the same  
 240 order of magnitude, i.e.  $[\eta] = 5.4$  L/kg for  $I = 0.1$  M, when Visser (1985) reported smaller intrinsic  
 241 viscosities for FA, i.e.  $[\eta]$  values around 1-2 L/kg for  $I = 0.1$  M.

242 Ratios  $\Delta V_D/V_D$  of the means of the difference between  $^{SRFA}V_D$  and  $^{Eu(III)-SRFA}V_D$  over the mean  $^{SRFA}V_D$   
 243 as a function of  $C_{SRFA}$  are presented in Figure 3.

$$\frac{\Delta V_D}{V_D} = \frac{\overline{^{SRFA}V_D} - \overline{^{Eu-SRFA}V_D}}{\overline{^{SRFA}V_D}} \quad (17)$$

244 The  $\Delta V_D/V_D$  ratio can be seen as a compression factor. One can clearly see that there is no significant  
 245 change in  $V_D$  with  $C_{SRFA}$  for Eu(III)-SRFA at  $C_{Eu(III)} = 1 \mu\text{M}$  compared to SRFA. In contrast, a  $C_{Eu(III)}$  of  
 246  $10 \mu\text{M}$  lead to a significant decrease in  $V_D$  values for  $C_{SRFA}$  smaller than  $100 \text{ mg}_{SRFA}/\text{L}$ —compression  
 247 factor reaches 50% for  $30 \text{ mg}_{SRFA}/\text{L}$ .

248 For a  $C_{\text{Eu}}$  of  $10 \mu\text{M}$ , Eu(III) is fully bound to SRFA for  $C_{\text{SRFA}}$  between 30 and 500  $\text{mg}_{\text{SRFA}}/\text{L}$  at pH  
 249 7—see NICA-Donnan simulations in Figure S1 of the supplementary information (SI). The total  
 250 number of sites of SRFA being  $7.74 \text{ mol/kg}$ , one can calculate that only 1.29; 0.43 and 0.26 % of SRFA  
 251 sites are occupied by  $\text{Eu}^{3+}$  respectively for  $C_{\text{SRFA}}$  of 100; 300 and 500  $\text{mg}_{\text{SRFA}}/\text{L}$ . At  $C_{\text{SRFA}}$  of 30 and 50  
 252  $\text{mg}_{\text{SRFA}}/\text{L}$ , 4.3 and 2.58 % of the SRFA sites are occupied by  $\text{Eu}^{3+}$ . At lower pH, the proportion of  
 253 SRFA sites occupied by Eu(III) are less important since Eu(III) is not fully bound to SRFA. At high  
 254  $C_{\text{SRFA}}$ , the complexes are behaving as pure fulvic since the amount of Eu(III) is too low to impact the  
 255 electrostatic, even though it is completely bound to SRFA. For the lowest  $C_{\text{SRFA}}$ , a higher amount of  
 256 the SRFA sites is occupied by  $\text{Eu}^{3+}$ , which lead to significant changes in the size and therefore impact  
 257 electrostatic parameters.

### 258 8.3 NICA-Donnan Calculations

259 Calculations are done using ECOSAT with mean values of  $V_D$  (Table 2a) calculated from TDA  
 260 experiments in order to test the sensitivity of this size parameter on NICA Donnan parameters. The  
 261 values of  $\chi$  are calculated for each  $C_{\text{SRFA}}$  using Eq (13) (Figure 4). The  $\chi_0$  value, corresponding to SRFA,  
 262 increases slightly from 24 to 32 for SRFA concentrations ranging from 30 to 500  $\text{mg}_{\text{SRFA}}/\text{L}$ . In contrast,  
 263  $\chi_{10}$ , corresponding to  $\text{Eu(III)}_{10 \mu\text{M}}\text{-SRFA}$ , is decreasing with  $C_{\text{SRFA}}$  from 44 to 27 for SRFA  
 264 concentrations ranging from 30 to 300  $\text{mg}_{\text{SRFA}}/\text{L}$ . For higher  $C_{\text{SRFA}}$ ,  $\chi_{10}$  values are close to the  $\chi_0$  ones.  
 265 In the presence of a metal, FA particles behave in a very different way. In presence of Eu(III),  $\chi_{10}$ , is  
 266 decreasing— $\psi_D$  increases according to Eq (9)—with  $C_{\text{SRFA}}$ . At low Eu/SRFA sites ratio – high  $C_{\text{SRFA}}$ —  
 267 the absolute value of the Donnan potential  $\psi_D$  decreases, and therefore, the repulsion between SRFA  
 268 particles can be less important and SRFA nanometric entities can approach and interact easily with  
 269 each other to form larger entities. We can consider these interactions between SRFA entities as  
 270 supramolecular associations of fulvic acid particles (Piccolo 2002, Kunhi Mouvenchery *et al.* 2012).

271 Ratios  $\chi_{10}/\chi_0$  for monovalent, divalent and trivalent cations calculated with ECOSAT are presented  
272 in Figure 5. These ratios are close to unity for  $C_{\text{SRFA}}$  of 300 and 500  $\text{mg}_{\text{SRFA}}/\text{L}$ , which mean that the  
273 Boltzmann factors are the same for SRFA particles and for SRFA complexes involving a mono, di or  
274 trivalent cation.  $C_{\text{SRFA}}$  is decreasing with  $\chi_{10}/\chi_0$  ratio—the greater increase is seen for SRFA complexes  
275 involving trivalent cations. The Boltzmann factor of  $\text{M}^{3+}$ -SRFA complexes is 6 times higher than the  
276 one of SRFA particles for a  $C_{\text{SRFA}}$  of 30  $\text{mg}_{\text{SRFA}}/\text{L}$  at pH 7. This evolution can here again be explained  
277 by the variation of the ratio of Eu bound to SRFA on SRFA sites. At a fixed  $C_{\text{Eu}}$ , the amount of SRFA  
278 sites that are occupied by Eu is more important at low  $C_{\text{SRFA}}$  than at high  $C_{\text{SRFA}}$ . The electrostatic is  
279 therefore more impacted at low  $C_{\text{SRFA}}$  when the ratio of Eu/SRFA sites is higher. Ratios  $\chi_{10}/\chi_0$  are  
280 evolving with pH. At a  $C_{\text{SRFA}}$  of 500  $\text{mg}_{\text{SRFA}}/\text{L}$ —low Eu/SRFA sites ratio—all the Eu is bound to SRFA  
281 for pH 4; 6 and 7 (Figure S1 of the SI). For lower  $C_{\text{SRFA}}$ —higher Eu/SRFA sites ratio—the proportion  
282 of Eu bound to SRFA is changing. At 30  $\text{mg}_{\text{SRFA}}/\text{L}$ , 45 % is bound at pH 4, 93 % at pH 6 and 99 % at  
283 pH 7 respectively. Since there is more Eu bound to SRFA with pH, the impact of Eu on electrostatics  
284 will be more important with pH.

#### 285 8.4 Environmental implications

286 Information on the structure of humic substances complexes with lanthanides(III), and more  
287 generally trivalent cations, is scarce. We evidence that Eu(III) interactions with natural organic matter  
288 impact the size and the electrostatic description of SRFA particles. Complexation and low Eu/SRFA  
289 sites ratio tend to lower the absolute value of the Donnan potential, which could favor a closer approach  
290 of the nanometric entities to form larger entities at higher scales. Particularly, one can remind that  
291 Plaschke *et al.* (2002) reported Eu(III)-induced agglomeration of HA at the 100 nm to micrometric  
292 scales, which could be interpreted as favored agglomeration of smaller entities in the framework of our  
293 measurements. This is a quite important observation since a Donnan volume in the NICA-Donnan  
294 model is determined by a relationship depending on ionic strength and  $b$ , which is an empirical

295 parameter determined from acid/base titrations. These titrations are done at quite high HS concentration  
296 (about 1 to 4 g/L) (Milne *et al.* 1995, Avena *et al.* 1999). Since these concentrations are not relevant  
297 of environmental conditions – about 1 to 10 mg/L of HS in lakes and rivers – and since the size of HS  
298 appears to be depending on HS concentration, and to decrease in the presence of a metal, the particle  
299 radius should be introduced in the model as an adjustable parameter.

300 One can suppose that other trivalent cations, e.g.  $\text{Fe}^{3+}$  and  $\text{Al}^{3+}$ , may share some commonalities, even  
301 if their chemistry are significantly different—e.g. higher charge to ionic radius ratio, stronger  
302 hydrolysis and lower solubility.

303 Iron is a major component at the surface of the Earth and therefore plays a central role in  
304 environmental surface systems. The speciation of Fe is an important issue in environmental science  
305 since it is involved in many biogeochemical cycles (Boyd and Ellwood 2010, Raiswell and Canfield  
306 2012). For instance, Nuzzo *et al.* (2013) evidenced changes of FA size with Fe(III) complexation –  
307 molecular size distribution of FA measured by HPSEC was increasing with Fe(III) complexation. As  
308 the calibration of HPSEC in Da using polysaccharides is not related to a metric size in Nuzzo *et al.*  
309 (2013) it is difficult to directly compare Da to nm. Nevertheless, even if this molecular size distribution  
310 evolution with metal concentration is in apparent contradiction with our observations on the Eu-SRFA  
311 system at the nanometric scale, it can be interpreted as the favored agglomeration of smaller entities,  
312 the Donnan potential of which sees its absolute value lowered and inter-particle repulsion decreased.  
313 Nuzzo *et al.* (2013) observed an opposite behavior for HA with Fe(III) complexation but at lower  
314 proportion of Fe(III) relative to HA, which renders the comparison between the two fractions difficult.  
315 Since Donnan volumes have shown to be dependent on metal/HS ratio, further studies are needed to  
316 confirm impact of other divalent ( $\text{Cu}^{2+}$ ,  $\text{Cd}^{2+}$ ...) and trivalent cations ( $\text{Fe}^{3+}$ ,  $\text{Al}^{3+}$ ...) on HS structures on  
317 a wider range of concentrations.

## 318 **9 Conclusion**

319 Sizes of SRFA and Eu(III)-SRFA complexes are on the nanometric scale and we cannot see any size  
320 evolution for a  $C_{Eu}$  of  $1 \mu M$ . For this concentration, Eu occupies less than 0.3 % of SRFA sites and  
321 thus, Eu(III)-SRFA complexes are behaving as pure fulvic acids. For a  $C_{Eu}$  of  $10 \mu M$  and at the lowest  
322  $C_{SRFA}$ , a higher amount of SRFA sites are occupied by Eu(III) which lead to significant changes in the  
323 size of complexes. The sizes seem thus to depend on metal/SRFA sites ratio. However, we cannot  
324 explain the different spatial organization of Eu-SRFA complexes perceived with SRFA concentration  
325 (Kouhail *et al.* 2016) by a variation in SRFA size. No important variations in  $R_H$  and NICA-Donnan  
326 parameters were seen for Eu(III)-SRFA complexes with a  $C_{Eu}$  of  $1 \mu M$  while the asymmetry ratio  
327 evolution in our previous study evidence the supramolecular associations of SRFA for these  
328 complexes. The supramolecular structures of SRFA perceived for Eu(III)-SRFA complexes with  $C_{Eu(III)}$   
329 of 1 and  $10 \mu M$  (Kouhail *et al.* 2016) cannot be evidence directly by  $R_H$  variations, but a comprehensive  
330 study of other NICA-Donnan parameters – i.e. the Boltzmann factor  $\chi$  and the Donnan potential  $\psi_D$  –  
331 brings new information on the structure of complexes. The possibility of an interfacial potential, as a  
332 double layer spreading outside the Donnan gel (Saito *et al.* 2005, Saito *et al.* 2009), should be  
333 investigated and implemented within the framework of NICA-Donnan. Counterion condensation in a  
334 double layer inside the particle in addition to the Donnan description, as recently proposed by Town  
335 and van Leeuwen (2016a, 2016b) seems to describe well the electrostatic interactions of divalent  
336 cations with HS.

337

338 Declaration of Funding This research did not receive any specific funding

339

340

341 **10 References**

- 342 Aiken GR, Malcolm RL (1987) Molecular weight of aquatic fulvic acids by vapor pressure osmometry.  
343 *Geochimica et Cosmochimica Acta* **51** (8), 2177-2184. DOI: 10.1016/0016-7037(87)90267-5
- 344 Aris R (1956) On the dispersion of a solute in a fluid flowing through a tube. *Proceedings of the Royal*  
345 *Society of London Series A: Mathematical, Physical and Engineering Sciences* **235** (1200), 67-77. DOI:  
346 10.1098/rspa.1956.0065
- 347 Avena MJ, Koopal LK, van Riemsdijk WH (1999) Proton binding to humic acids: electrostatic and  
348 intrinsic interactions. *Journal of Colloid and Interface Science* **217** (1), 37-48. DOI:  
349 10.1006/jcis.1999.6317
- 350 Baalousha M, Lead JR (2007) Characterization of natural aquatic colloids (< 5 nm) by flow-field flow  
351 fractionation and atomic force microscopy. *Environmental Science & Technology* **41** (4), 1111-1117.  
352 DOI: 10.1021/es061766n
- 353 Benedetti M, Ranville JF, Ponthieu M, Pinheiro JP (2002) Field-flow fractionation characterization  
354 and binding properties of particulate and colloidal organic matter from the Rio Amazon and Rio Negro.  
355 *Organic Geochemistry* **33** (3), 269-279. DOI: 10.1016/S0146-6380(01)00159-0
- 356 Benedetti MF, van Riemsdijk WH, Koopal LK (1996) Humic substances considered as a  
357 heterogeneous Donnan gel phase. *Environmental Science & Technology* **30** (6), 1805-1813. DOI:  
358 10.1021/Es950012y
- 359 Bouby M, Geckeis H, Lützenkirchen J, Mihai S, Schäfer T (2011) Interaction of bentonite colloids  
360 with Cs, Eu, Th and U in presence of humic acid: a flow field-flow fractionation study. *Geochimica et*  
361 *Cosmochimica Acta* **75** (13), 3866-3880. DOI: 10.1016/j.gca.2011.04.015
- 362 Bouby M, Ngo Manh T, Geckeis H, Scherbaum FJ, Kim J-I (2002) Characterization of aquatic colloids  
363 by a combination of LIBD and ICP-MS following the size fractionation. *Radiochimica Acta* **90** (9-  
364 11/2002), 727-732. DOI: 10.1524/ract.2002.90.9-11\_2002.727
- 365 Boyd PW, Ellwood MJ (2010) The biogeochemical cycle of iron in the ocean. *Nature Geoscience* **3**  
366 (10), 675-682. DOI: 10.1038/ngeo964
- 367 Bryan ND, Abrahamsen L, Evans N, Warwick P, Buckau G, Weng LP, van Riemsdijk WH (2012) The  
368 effects of humic substances on the transport of radionuclides: recent improvements in the prediction of  
369 behaviour and the understanding of mechanisms. *Applied Geochemistry* **27** (2), 378-389. DOI:  
370 10.1016/j.apgeochem.2011.09.008
- 371 Chin Y-P, Aiken G, O'Loughlin E (1994) Molecular weight, polydispersity, and spectroscopic  
372 properties of aquatic humic substances. *Environmental Science & Technology* **28** (11), 1853-1858.  
373 DOI: 10.1021/es00060a015
- 374 d'Orlyé F, Reiller PE (2012) Contribution of capillary electrophoresis to an integrated vision of humic  
375 substances size and charge characterizations. *Journal of Colloid and Interface Science* **368** (1), 231-  
376 240. DOI: 10.1016/j.jcis.2011.11.046
- 377 d'Orlyé F, Varenne A, Gareil P (2008) Determination of nanoparticle diffusion coefficients by Taylor  
378 dispersion analysis using a capillary electrophoresis instrument. *Journal of Chromatography A* **1204**  
379 (2), 226-232. DOI: 10.1016/j.chroma.2008.08.008
- 380 de Levie R (2004) 'Advanced Excel for Scientific Data Analysis.' (Oxford University Press, USA)
- 381 De Wit JCM, van Riemsdijk WH, Nederlof MM, Kinniburgh DG, Koopal LK (1990) Analysis of ion  
382 binding on humic substances and the determination of intrinsic affinity distributions. *Analytica*  
383 *Chimica Acta* **232**, 189-207. DOI: 10.1016/S0003-2670(00)81235-0
- 384 Diallo MS, Glinka CJ, Goddard III WA, Johnson Jr JH (2005) Characterization of nanoparticles and  
385 colloids in aquatic systems 1. Small angle neutron scattering investigations of Suwannee River fulvic  
386 acid aggregates in aqueous solutions. *Journal of Nanoparticle Research* **7** (4-5), 435-448. DOI:  
387 10.1007/s11051-005-7524-4

- 388 Domingos RF, Tufenkji N, Wilkinson KJ (2009) Aggregation of titanium dioxide nanoparticles: role  
389 of a fulvic acid. *Environmental Science & Technology* **43** (5), 1282-1286. DOI: 10.1021/es8023594
- 390 Ghosh K, Schnitzer M (1980) Macromolecular structures of humic substances. *Soil Science* **129** (5),  
391 266-276. DOI: 10.1097/00010694-198005000-00002
- 392 Hosse M, Wilkinson KJ (2001) Determination of electrophoretic mobilities and hydrodynamic radii of  
393 three humic substances as a function of pH and ionic strength. *Environmental Science & Technology*  
394 **35** (21), 4301-4306. DOI: 10.1021/es010038r
- 395 Hummel W, Berner U, Curti E, Pearson FJ, Thoenen T (2002) Nagra/PSI Chemical Thermodynamic  
396 Data Base 01/01. NAGRA Technical Report Number NTB 02-06, Parkland, FL, USA.
- 397 Hummel W, Glaus MA, van Loon LR (2000) Trace metal-humate interactions. II. The “conservative  
398 roof” model and its application. *Applied Geochemistry* **15** (7), 975-1001. DOI: 10.1016/S0883-  
399 2927(99)00100-6
- 400 Kawahigashi M, Sumida H, Yamamoto K (2005) Size and shape of soil humic acids estimated by  
401 viscosity and molecular weight. *Journal of Colloid and Interface Science* **284** (2), 463-469. DOI:  
402 10.1016/j.jcis.2004.10.023
- 403 Keizer MG, van Riemsdijk WH (1994) A computer program for the calculation of chemical speciation  
404 and transport in soil-water systems (ECOSAT 4.7). Wageningen Agricultural University, Wageningen,  
405 The Netherlands.
- 406 Kinniburgh DG, van Riemsdijk WH, Koopal LK, Borkovec M, Benedetti MF, Avena MJ (1999) Ion  
407 binding to natural organic matter: competition, heterogeneity, stoichiometry and thermodynamic  
408 consistency. *Colloids and Surfaces A: Physicochemical and Engineering Aspects* **151** (1-2), 147-166.  
409 DOI: 10.1016/S0927-7757(98)00637-2
- 410 Kouhail YZ, Benedetti MF, Reiller PE (2016) Eu(III)-Fulvic Acid Complexation: Evidence of Fulvic  
411 Acid Concentration Dependent Interactions by Time-Resolved Luminescence Spectroscopy.  
412 *Environmental Science & Technology* **50** (7), 3706-3713. DOI: 10.1021/acs.est.5b05456
- 413 Kunhi Mouvenchery Y, Kučerík J, Diehl D, Schaumann GE (2012) Cation-mediated cross-linking in  
414 natural organic matter: a review. *Reviews in Environmental Science and Bio/Technology* **11** (1), 41-54.  
415 DOI: 10.1007/s11157-011-9258-3
- 416 Lead JR, Wilkinson KJ, Starchev K, Canonica S, Buffle J (2000) Determination of diffusion  
417 coefficients of humic substances by fluorescence correlation spectroscopy: role of solution conditions.  
418 *Environmental Science & Technology* **34** (7), 1365-1369. DOI: 10.1021/es9907616
- 419 McCarthy JF, Czerwinski KR, Sanford WE, Jardine PM, Marsh JD (1998a) Mobilization of transuranic  
420 radionuclides from disposal trenches by natural organic matter. *Journal of Contaminant Hydrology* **30**  
421 (1-2), 49-77. DOI: 10.1016/S0169-7722(97)00032-6
- 422 McCarthy JF, Sanford WE, Stafford PL (1998b) Lanthanide field tracers demonstrate enhanced  
423 transport of transuranic radionuclides by natural organic matter. *Environmental Science & Technology*  
424 **32** (24), 3901-3906. DOI: 10.1021/Es971004f
- 425 Milne CJ, Kinniburgh DG, de Wit JCM, van Riemsdijk WH, Koopal LK (1995) Analysis of proton  
426 binding by a peat humic acid using a simple electrostatic model. *Geochimica et Cosmochimica Acta*  
427 **59** (6), 1101-1112. DOI: 10.1016/0016-7037(95)00027-W
- 428 Milne CJ, Kinniburgh DG, Tipping E (2001) Generic NICA-Donnan model parameters for proton  
429 binding by humic substances. *Environmental Science & Technology* **35** (10), 2049-2059. DOI:  
430 10.1021/es000123j
- 431 Milne CJ, Kinniburgh DG, van Riemsdijk WH, Tipping E (2003) Generic NICA-Donnan model  
432 parameters for metal-ion binding by humic substances. *Environmental Science & Technology* **37** (5),  
433 958-971. DOI: 10.1021/es0258879

- 434 Moulin V, Reiller P, Amekraz B, Moulin C (2001) Direct characterization of iodine covalently bound  
435 to fulvic acids by electrospray mass spectrometry. *Rapid Communications in Mass Spectrometry* **15**  
436 (24), 2488-2496. DOI: 10.1002/rcm.503
- 437 Naber A, Plaschke M, Rothe J, Hofmann H, Fanghänel T (2006) Scanning transmission X-ray and  
438 laser scanning luminescence microscopy of the carboxyl group and Eu(III) distribution in humic acid  
439 aggregates. *Journal of Electron Spectroscopy and Related Phenomena* **153** (3), 71-74. DOI:  
440 10.1016/j.elspec.2006.06.005
- 441 Nuzzo A, Sánchez A, Fontaine B, Piccolo A (2013) Conformational changes of dissolved humic and  
442 fulvic superstructures with progressive iron complexation. *Journal of Geochemical Exploration* **129**,  
443 1-5. DOI: 10.1016/j.gexplo.2013.01.010
- 444 Österberg R, Szajdak L, Mortensen K (1994) Temperature-dependent restructuring of fractal humic  
445 acids: a proton-dependent process. *Environment International* **20** (1), 77-80. DOI: 10.1016/0160-  
446 4120(94)90069-8
- 447 Peuravuori J, Bursakova P, Pihlaja K (2007) ESI-MS analyses of lake dissolved organic matter in light  
448 of supramolecular assembly. *Analytical and Bioanalytical Chemistry* **389** (5), 1559-1568. DOI:  
449 10.1007/s00216-007-1553-z
- 450 Peuravuori J, Pihlaja K (1997) Molecular size distribution and spectroscopic properties of aquatic  
451 humic substances. *Analytica Chimica Acta* **337** (2), 133-149. DOI: 10.1016/S0003-2670(96)00412-6
- 452 Piccolo A (2002) The supramolecular structure of humic substances: a novel understanding of humus  
453 chemistry and implications in soil science. *Advances in Agronomy* **75**, 57-134. DOI: 10.1016/S0065-  
454 2113(02)75003-7
- 455 Piccolo A, Spiteller M (2003) Electrospray ionization mass spectrometry of terrestrial humic  
456 substances and their size fractions. *Analytical and Bioanalytical Chemistry* **377** (6), 1047-1059. DOI:  
457 10.1007/s00216-003-2186-5
- 458 Plancque G, Amekraz B, Moulin V, Toulhoat P, Moulin C (2001) Molecular structure of fulvic acids  
459 by electrospray with quadrupole time-of-flight mass spectrometry. *Rapid Communications in Mass*  
460 *Spectrometry* **15** (10), 827-835. DOI: 10.1002/rcm.307
- 461 Plaschke M, Rothe J, Denecke MA, Fanghänel T (2004) Soft X-ray spectromicroscopy of humic acid  
462 europium(III) complexation by comparison to model substances. *Journal of Electron Spectroscopy and*  
463 *Related Phenomena* **135** (1), 53-62. DOI: 10.1016/j.elspec.2003.12.007
- 464 Plaschke M, Rothe J, Schäfer T, Denecke MA, Dardenne K, Pompe S, Heise KH (2002) Combined  
465 AFM and STXM in situ study of the influence of Eu(III) on the agglomeration of humic acid. *Colloids*  
466 *and Surfaces A: Physicochemical and Engineering Aspects* **197** (1-3), 245-256. DOI: 10.1016/S0927-  
467 7757(01)00901-3
- 468 Raiswell R, Canfield DE (2012) The iron biogeochemical cycle past and present. *Geochemical*  
469 *Perspectives* **1** (1), 1-2. DOI: 10.7185/geochempersp.1.1
- 470 Saito T, Koopal LK, Nagasaki S, Tanaka S (2009) Electrostatic potentials of humic acid: Fluorescence  
471 quenching measurements and comparison with model calculations. *Colloids and Surfaces A:*  
472 *Physicochemical and Engineering Aspects* **347** (1-3), 27-32. DOI: 10.1016/j.colsurfa.2008.10.038
- 473 Saito T, Nagasaki S, Tanaka S, Koopal LK (2005) Electrostatic interaction models for ion binding to  
474 humic substances. *Colloids and Surfaces A: Physicochemical and Engineering Aspects* **265** (1-3), 104-  
475 113. DOI: 10.1016/j.colsurfa.2004.10.139
- 476 Sutton R, Sposito G (2005) Molecular structure in soil humic substances: the new view. *Environmental*  
477 *Science & Technology* **39** (23), 9009-9015. DOI: 10.1021/es050778q
- 478 Taylor G (1953) Dispersion of soluble matter in solvent flowing slowly through a tube. *Proceedings*  
479 *of the Royal Society of London Series A: Mathematical, Physical and Engineering Sciences* **219** (1137),  
480 186-203. DOI: 10.1098/rspa.1953.0139

- 481 Tesfa M, Duval JFL, Marsac R, Dia A, Pinheiro JP (2022) Absolute and relative positioning of natural  
482 organic matter acid-base potentiometric titration curves: implications for the evaluation of the density  
483 of charged reactive sites. *Environmental Science & Technology* DOI: 10.1021/acs.est.2c00828 DOI:  
484 10.1021/acs.est.2c00828
- 485 Tipping E (1998) Humic ion-binding model VI: an improved description of the interactions of protons  
486 and metal ions with humic substances. *Aquatic Geochemistry* **4** (1), 3-47. DOI:  
487 10.1023/A:1009627214459
- 488 Tipping E, Lofts S, Sonke JE (2011) Humic ion-binding Model VII: a revised parameterisation of  
489 cation-binding by humic substances. *Environmental Chemistry* **8** (3), 225-235. DOI: 10.1071/EN11016
- 490 Town RM, van Leeuwen HP (2016a) Intraparticulate speciation analysis of soft nanoparticulate metal  
491 complexes. The impact of electric condensation on the binding of Cd<sup>2+</sup>/Pb<sup>2+</sup>/Cu<sup>2+</sup> by humic acids.  
492 *Physical Chemistry Chemical Physics* **18** (15), 10049-10058. DOI: 10.1039/C6CP01229A
- 493 Town RM, van Leeuwen HP (2016b) Metal ion-humic acid nanoparticle interactions: role of both  
494 complexation and condensation mechanisms. *Physical Chemistry Chemical Physics* **18** (27), 18024-  
495 18032. DOI: 10.1039/C6CP02634F
- 496 Visser SA (1985) Viscosimetric studies on molecular weight fractions of fulvic and humic acids of  
497 aquatic, terrestrial and microbial origin. *Plant and Soil* **87** (2), 209-221.
- 498 von Wandruszka R, Ragle C, Engebretson R (1997) The role of selected cations in the formation of  
499 pseudomicelles in aqueous humic acid. *Talanta* **44**, 805-809. DOI: 10.1016/s0039-9140(96)02116-9
- 500 Acknowledgement : This paper forms part of the PhD thesis of Yasmine Kouhail (2016)

## 501 **11 Conflict of Interest**

502 *The authors declare that the research was conducted in the absence of any commercial or financial*  
503 *relationships that could be construed as a potential conflict of interest.*

504 Data Availability Statement : data will be made available upon request to the corresponding author.

505

## 506 12 Tables

507 **Table 1.** NICA Donnan parameters for proton and Eu(III) binding to a fulvic acid (Milne *et al.* 2003).

	<b>Q<sub>1</sub></b> (mol.kg <sub>FA</sub> <sup>-1</sup> )	<b>n<sub>1,M</sub></b>	<b>log<sub>10</sub>K<sub>1,M</sub><sup>-</sup></b>	<b>p<sub>1</sub></b>	<b>Q<sub>2</sub></b> (mol.kg <sub>FA</sub> <sup>-1</sup> )	<b>n<sub>2,M</sub></b>	<b>log<sub>10</sub>K<sub>2,M</sub><sup>-</sup></b>	<b>p<sub>2</sub></b>	<b>B</b>
<b>H<sup>+</sup></b>	5.88	0.66	2.34	0.59	1.86	0.76	8.60	0.70	0.57
<b>Eu<sup>3+</sup></b>		0.47	-1.92			0.45	5.87		

508

509 **Table 2.** Donnan volumes of SRFA particles ( $^{SRFA}V_D$ ) and Eu-SRFA ( $^{Eu-SRFA}V_D$ ) complexes  
 510 calculated using Eq. (14) with  $R = R_H$  (Table 2a) or  $R = R_H + \kappa^{-1}$  (Table 2b), and  $\rho_{HS} = 2.17$  and  $M_w =$   
 511  $829$  g/mol.

(a)  $V_D (R_H)$  L/kg

	$C_{SRFA}$ (mg/L)	SRFA $V_D$ (L/kg)	Eu <sub>1</sub> $\mu$ M-SRFA $V_D$ (L/kg)	Eu <sub>10</sub> $\mu$ M-SRFA $V_D$ (L/kg)
	pH 4	30	1.82	1.88
50		2.37	2.16	1.49
100		2.43	1.64	1.78
300		2.34	1.97	2.36
500		1.92	1.80	1.78
pH 6	30	2.50	2.67	1.08
	50	2.34	2.43	1.50
	100	2.39	2.47	1.81
	300	2.40	2.31	1.97
	500	1.88	1.88	1.68
pH 7	30	2.70	2.49	1.25
	50	2.56	2.90	1.58
	100	2.42	2.56	1.81
	300	2.17	2.14	2.01
	500	1.64	1.75	1.66

512

(b)  $V_D (R_H + \kappa^{-1})$  L/kg

	$C_{SRFA}$ (mg/L)	SRFA $V_D$ (L/kg)	Eu <sub>1</sub> $\mu$ M-SRFA $V_D$ (L/kg)	Eu <sub>10</sub> $\mu$ M-SRFA $V_D$ (L/kg)
	pH 4	30	19.7	20.0
50		22.0	21.1	18.3
100		22.2	18.9	19.6
300		21.9	20.4	22.0
500		20.2	19.7	19.5
pH 6	30	22.5	23.2	16.4
	50	21.9	22.2	18.3
	100	22.1	22.4	19.7
	300	22.1	21.7	20.4
	500	20.0	20.0	19.1
pH 7	30	23.3	22.5	17.2
	50	22.8	24.0	18.7
	100	22.2	22.7	19.7
	300	21.2	21.1	20.6
	500	19.0	19.4	19.0

513

514

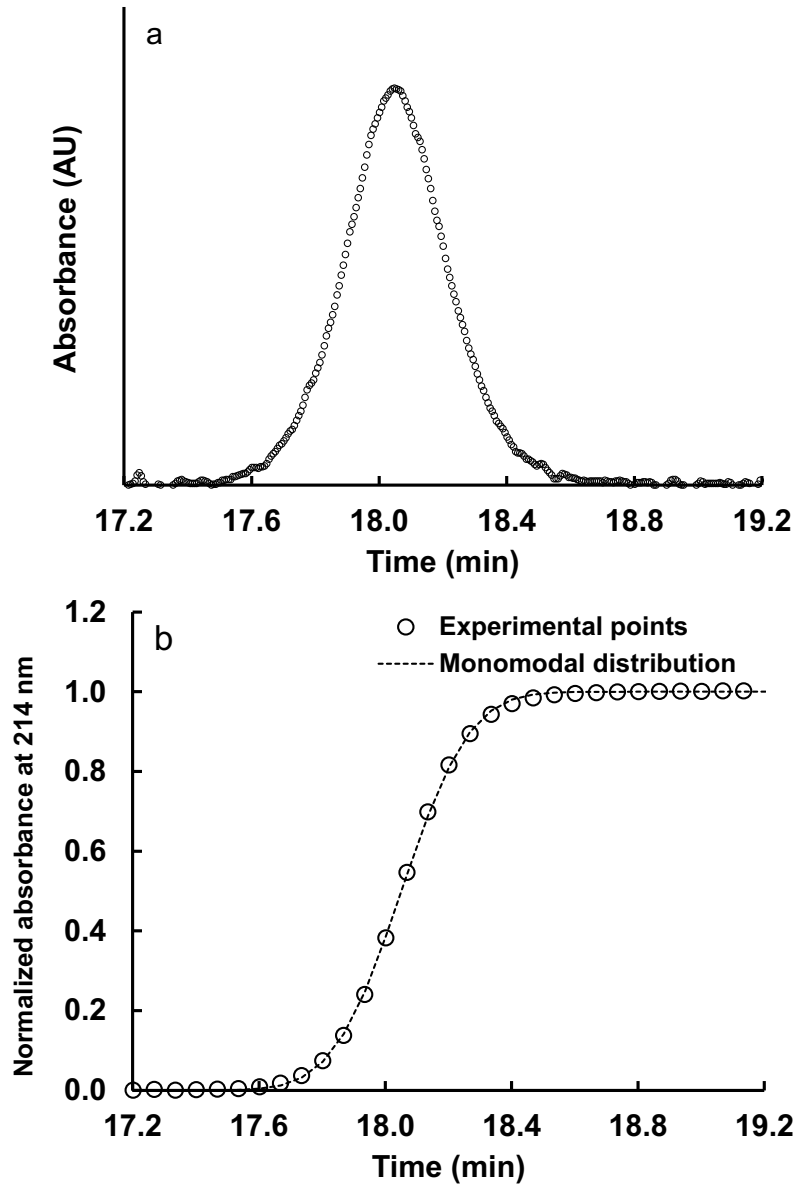


**Figure 1.** (a) Taylogram of Eu-SRFA complex at pH 4,  $C_{Eu} = 1 \mu\text{M}$  and  $C_{SRFA} = 100 \text{ mg}_{SRFA}/\text{L}$  and (b) Experimental front concentration profile (one-tenth of the experimental points are represented); dotted line is the fit of the analytical solution to the convection–diffusion Eq **Erreur ! Source du renvoi introuvable.** assuming a mono-modal distribution: Experimental conditions: fused-silica capillary,  $50 \mu\text{m}$  id  $\times$  60.8 cm (detection length 52.6 cm); mobilization pressure 50 mbar; temperature 25 °C; UV detection 214 nm.

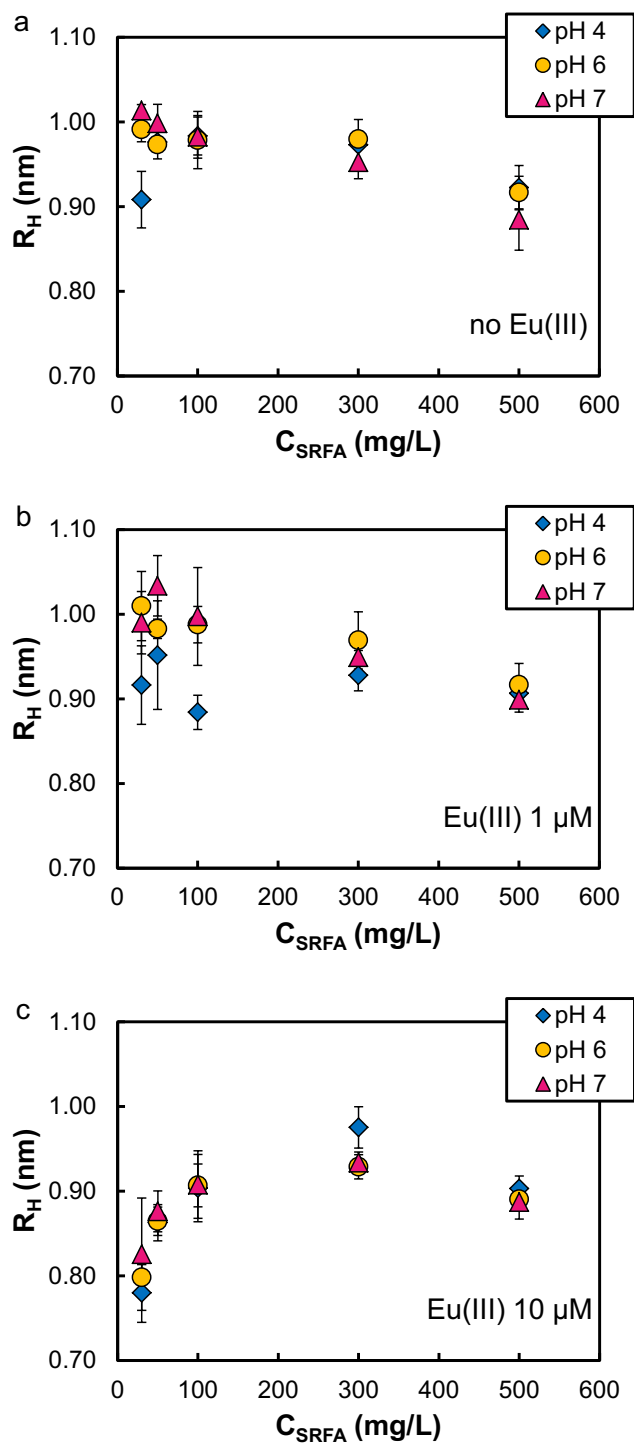


**Figure 2.** Hydrodynamic radii ( $R_H$ ) as function of  $C_{SRFA}$  for SRFA samples (a) and Eu(III)-SRFA complexes, for  $C_{Eu}$  of 1 (b) and 10  $\mu$ M (c), at pH 4 (blue diamonds), 6 (yellow circles), and 7 (pink triangles). Viscosity used for calculation is 0.00089 kg.s<sup>-1</sup>.m<sup>-1</sup>. Error bars represent  $2\sigma$  on 3 runs of the sample.  $R_H$  values are also given in Table S1 in the supplementary information.

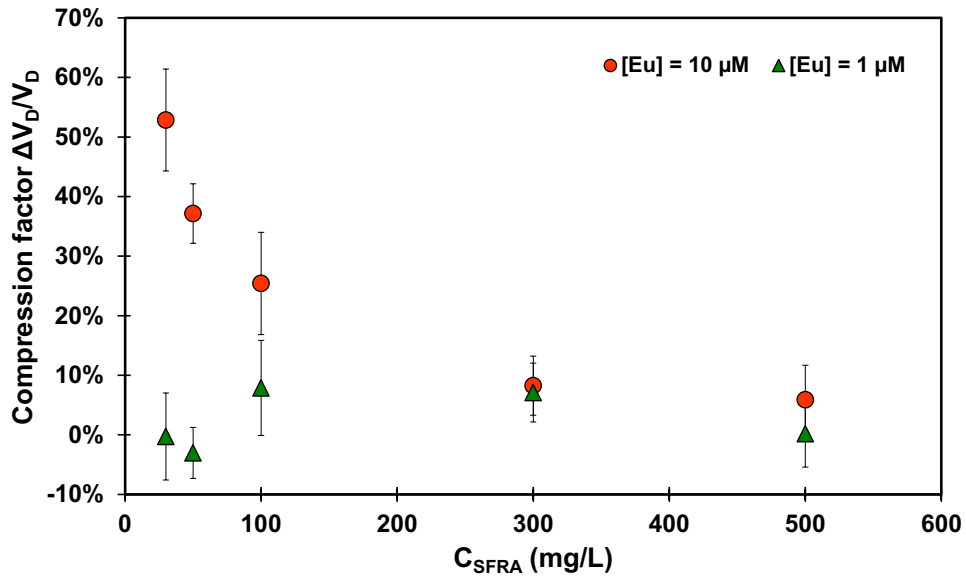


**Figure 3.** Evolution of the compression factor  $\Delta V_D/V_D$  as function of  $C_{SFRA}$  for  $[Eu] = 10 \mu M$  (orange circles) and  $[Eu] = 1 \mu M$  (green triangles).

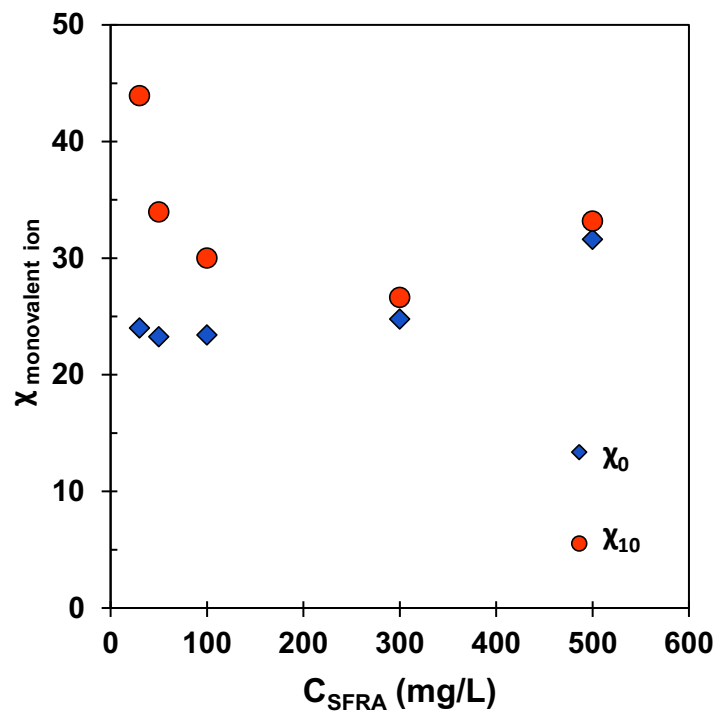


**Figure 4.** Boltzmann factor  $\chi$  calculated with ECOSAT (using NICA-Donnan generic parameters for fulvic acids) for a monovalent ion, for SRFA particles ( $\chi_0$ ) in blue diamonds and for Eu(III)<sub>10μM</sub>-SRFA complexes ( $\chi_{10}$ ) in orange circles as function of  $C_{SFRA}$ .

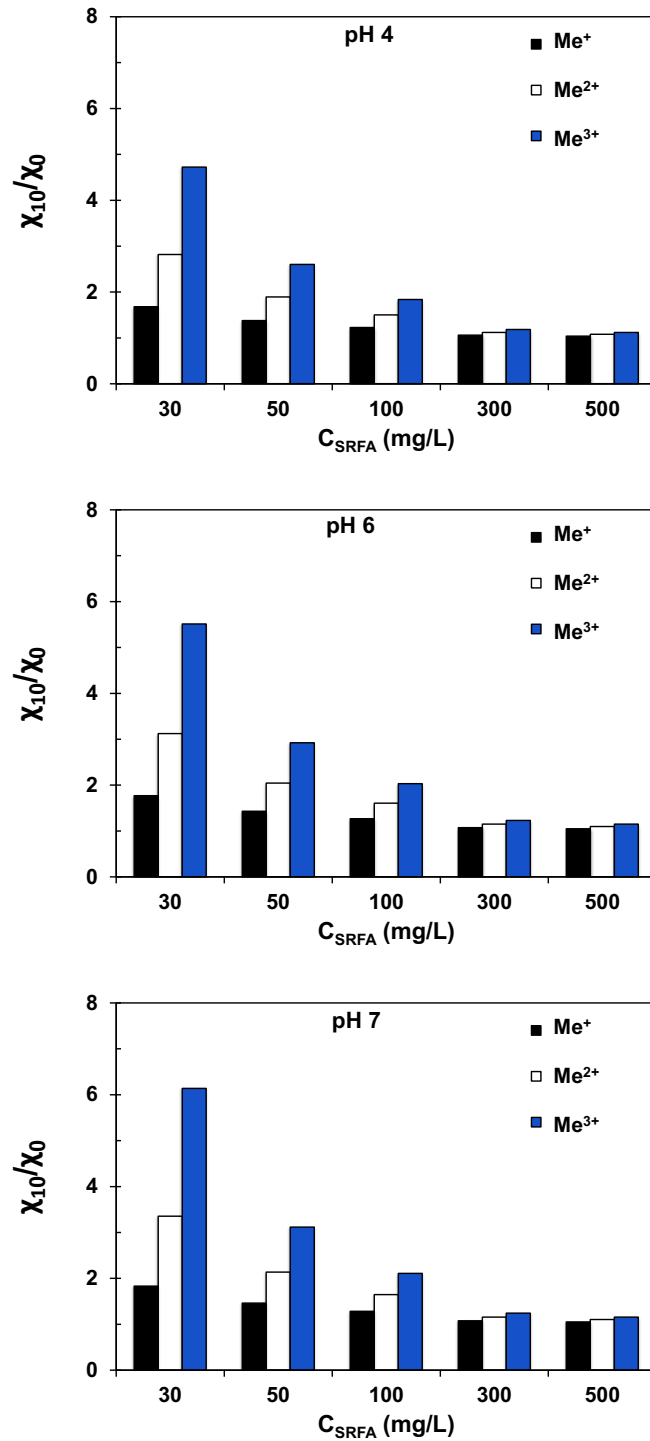


**Figure 5.** Ratio of the Boltzmann factor  $\chi_{10}$  calculated with ECOSAT for  $Eu(III)_{10\mu M}$ -SRFA complexes at pH 4, 6 and 7 on the Boltzmann factor  $\chi_0$  for SRFA particles as function of SRFA concentration for monovalent (in black), divalent (in white) and trivalent (in blue) cations.

## Supplementary data:

### **Size evolution of Eu(III)-fulvic acid complexes with pH, metal, and fulvic acid concentrations: implications for modelling of metal-humic substances interactions.**

**Yasmine Kouhail<sup>1,2\*</sup>, Pascal E. Reiller<sup>1</sup>, Laurent Vio<sup>1,3</sup>, Marc F. Benedetti<sup>2</sup>**

<sup>1</sup> Université Paris-Saclay, CEA, Service d'Etudes Analytiques et de Réactivité des Surfaces (SEARS), F-91191, Gif-sur-Yvette, France.

<sup>2</sup> Institut de Physique du Globe de Paris, Sorbonne Paris Cité, Université Paris Diderot, UMR 7154 CNRS, F-75005 Paris, France.

<sup>3</sup> Present address: CEA, DG/CEACAD/D3S/SPR/LANSE, Cadarache, Saint-Paul-lès-Durance Cedex, France

#### **\*Correspondence:**

Yasmine Kouhail

yasmine.kouhail@kit.edu

Present address: Karlsruher Institut für Technologie (KIT), Institut für Nukleare Entsorgung (INE), Hermann-von-Helmholtz Platz 1, D-76344 Eggenstein-Leopoldshafen, Germany

The supplementary data contains one Figure and one Table. The Figure shows the simulation of the proportion of Eu(III) bound to a generic fulvic acid for  $C_{\text{Eu(III)}}$  of 1  $\mu\text{M}$  and 10  $\mu\text{M}$  at pH 4, 6, and 7, using generic NICA-Donnan parameters. The Table shows the hydrodynamic radii as function of  $C_{\text{SRFA}}$  for SRFA samples and Eu(III)-SRFA complexes, for  $C_{\text{Eu}}$  of 1 and 10  $\mu\text{M}$ , at pH 4, 6, and 7.

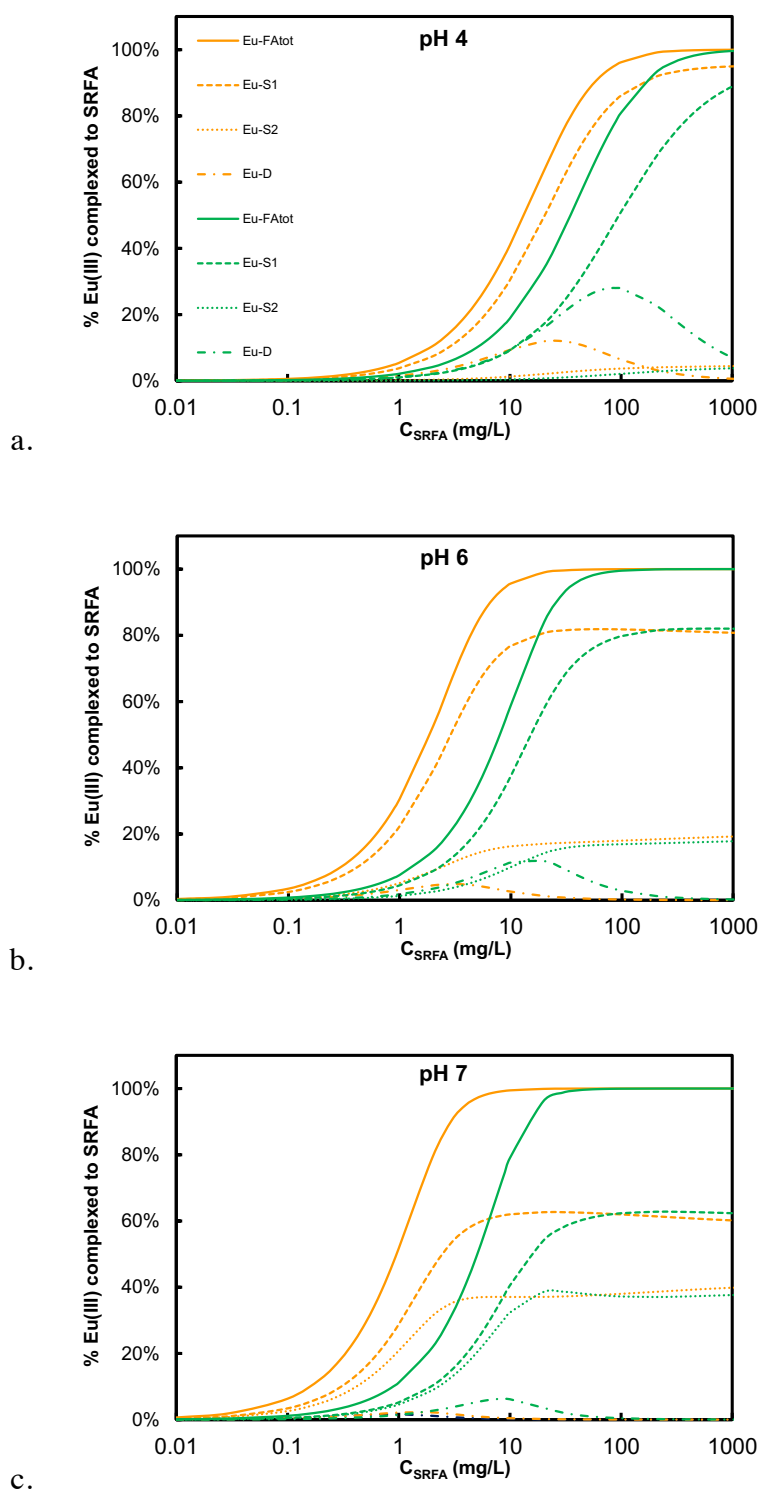


Figure S1. Simulation of the proportion of Eu(III) bound to a generic fulvic acid for  $C_{Eu(III)}$  of 1  $\mu$ M (orange lines) and 10  $\mu$ M (green lines) at pH 4 (a), 6 (b), and 7 (c). Simulation of Eu(III) distribution on S<sub>1</sub> sites (dashed lines) and S<sub>2</sub> sites (dotted lines) of SRFA. Solid lines are the sum of S<sub>1</sub> and S<sub>2</sub> sites. Generic NICA-Donnan parameters are given in Table 1.

Table S1. Hydrodynamic radii ( $R_H$ ) as function of  $C_{SRFA}$  for SRFA samples and Eu(III)-SRFA complexes, for  $C_{Eu}$  of 1 and 10  $\mu\text{M}$ , at pH 4, 6, and 7. Viscosity used for calculation is 0.00089  $\text{kg}\cdot\text{s}^{-1}\cdot\text{m}^{-1}$ .

$R_H$  (nm)

	$C_{SRFA}$ (mg/L)	SRFA $R_H$ (nm)	Eu <sub>1</sub> $\mu\text{M}$ -SRFA $R_H$ (nm)	Eu <sub>10</sub> $\mu\text{M}$ -SRFA $R_H$ (nm)
<b>pH 4</b>	<b>30</b>	0.91	0.92	0.78
	<b>50</b>	0.98	0.95	0.86
	<b>100</b>	0.98	0.88	0.90
	<b>300</b>	0.97	0.93	0.98
	<b>500</b>	0.92	0.91	0.90
<b>pH 6</b>	<b>30</b>	0.99	1.01	0.80
	<b>50</b>	0.97	0.98	0.86
	<b>100</b>	0.98	0.99	0.91
	<b>300</b>	0.98	0.97	0.93
	<b>500</b>	0.92	0.92	0.89
<b>pH 7</b>	<b>30</b>	1.01	0.99	0.83
	<b>50</b>	1.00	1.03	0.88
	<b>100</b>	0.98	1.00	0.91
	<b>300</b>	0.95	0.95	0.93
	<b>500</b>	0.88	0.90	0.89